Available online at www.sciencedirect.com
ScienceDirect
Journal of Photochemistry and Photobiology A: Chemistry 193 (2008) 213–221
Journal of Photochemistry and Photobiology A:Chemistry
www.elsevier.com/locate/jphotochem

$InVO_4$-sensitized TiO_2 photocatalysts for efficient air purification with visible light

Guangcan Xiao, Xinchen Wang, Danzhen Li, Xianzhi Fu *

Research Institute of Photocatalysis, Chemistry & Chemical Engineering College, Fuzhou University, Fuzhou 350002, China

Received 22 November 2006; received in revised form 28 March 2007; accepted 27 June 2007
Available online 30 June 2007

Abstract

A visible-light-driven $InVO_4/TiO_2$ mesoporous photocatalyst was prepared by a sol–gel method. The catalyst was characterized by powder X-ray diffraction (XRD), nitrogen adsorption–desorption, transmission electron microscopy (TEM), UV-vis diffuse reflectance spectroscopy, X-ray photoelectron spectra (XPS), ultraviolet photoelectron spectra (UPS), and spin-trapping electron paramagnetic resonance (EPR). Photocatalytic activity of the sample was evaluated by the degradation of volatile organic compounds (VOCs) in air under visible light irradiation ($450\,nm \leq \lambda \leq 900\,nm$). Results revealed that the addition of $InVO_4$ leaded to the visible light response up to ~540 nm for $InVO_4/TiO_2$. Moreover, upon visible light irradiation, some superoxide radical anions, such as $O_2^{\bullet -}$ and $OH^{\bullet}$ radicals, were generated on $InVO_4/TiO_2$, leading to the decomposition of VOCs. The high photocatalytic activity towards VOCs (e.g. benzene) was still maintained in the cycle experiments, and the turnover numbers recorded within 12 h work out to be 11.8 mol (produced CO_2) and 6.2 mol (degraded C_6H_6) per mol catalyst. Deactivation of the photocatalyst was not observed during the cycle experiments. It has been confirmed that $InVO_4/TiO_2$ photocatalyst could be activated by visible light due to the existence of the $InVO_4$. Based on the energy-band levels of $InVO_4$ and TiO_2, a photosensitization mechanism of $InVO_4/TiO_2$ is proposed.

Keywords: Photocatalysis; Visible light; Sensitization; $InVO_4/TiO_2$; Environmental purification

1. Introduction

Semiconductor-mediated photocatalysis is one of the most efficient destructive technologies among advanced oxidation processes (AOPs) for environmental remediation [1–2]. TiO_2 has been intensively investigated as a semiconductor photocatalyst because of its stability, cheapness and environmental friendliness. Unfortunately, a major obstacle in the popularization of this semiconductor material is the large band gap, 3.2 eV for bulk TiO_2. This severe disadvantage limits the photocatalyst photosensitivity to the ultraviolet region, a small fraction (~5%) of the solar energy. Therefore, significant efforts have been devoted to developing stable and efficient photocatalysts capable of using abundant visible light in solar spectrum or artificial light sources [3–9].

For this purpose, doping TiO_2 with various noble/transition metal or metal ions and their photocatalytic activities has been investigated extensively [10–13]. Some theoretical calculations have also been carried out to suggest that anion doping of TiO_2 has a considerable effect on the band gap alteration [5]. However, the photocatalytic activity of metal ions doping is impaired by thermal instability and an increase in carrier-recombination facilities. Few of them gave prospective satisfactory results. Photosensitization is another approach to extend the photosensitivity of TiO_2 into visible region. Excited by visible light, sensitizer adsorbed on TiO_2 injects electron into the conduction band (CB) of TiO_2, which acts as a mediator for transferring electrons from the excited sensitizer to the electron acceptors on TiO_2 surface. Traditional sensitizers are small band-gap semiconductors or organic dyes. Some of these systems have achieved high quantum efficiencies [14,15]. However, the sensitized systems inevitably lose their light-responsive functions due to the photocorrosion/photodegradation of sensitizers, making the overall process impractical. The key challenge in sensitization-type photocatalysis is therefore finding sufficiently stable sensitizers with appropriate electronic states.

Stable multimetallic oxides (e.g. $InMO_4$ [M = V, Nb, or Ta]) have recently attracted much attention as new photocatalytic

* Corresponding author. Fax: +86 591 83738608.
E-mail address: xzfu@fzu.edu.cn (X. Fu).

1010-6030/$ – see front matter © 2007 Elsevier B.V. All rights reserved.
doi:10.1016/j.jphotochem.2007.06.027

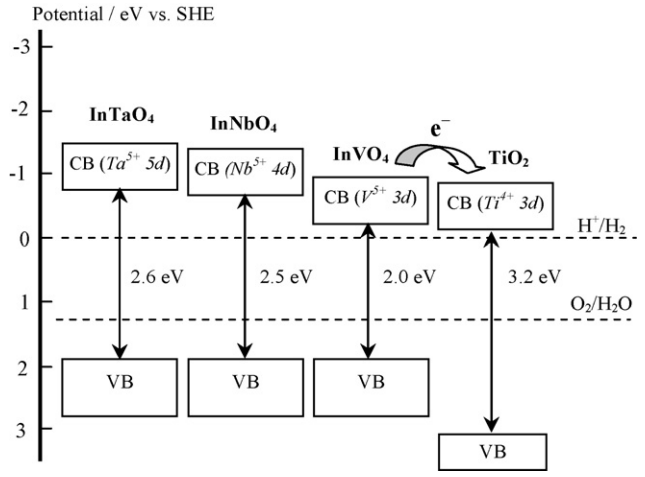

Scheme 1. Proposed band structures of $InMO_4$ and TiO_2. The energy levels of Ta^{5+}5d, Nb^{5+}4d, or V^{5+}3d are more negative than that of Ti^{4+}3d. Therefore, electron transfer from the conduction band of $InMO_4$ to that of TiO_2 is allowed.

materials for hydrogen generation from water splitting under visible light irradiation [3,16–18]. The electronic structures calculated from density functional theory (DFT) show that the d orbital of the transition metals in $InMO_4$ form the bottom of the conduction bands, and the top of the valence band consist of O2p orbital (Scheme 1) [19]. Normally, in single component metal oxides (e.g. TiO_2), the energy level of O2p orbital is located at about +3 eV versus SHE. The band gap energy between the metal-d and O2p-levels is therefore too wide to absorb visible light. In the case of $InMO_4$, the valence band energy from O2p-level of the polyhedrons is ca. 1.0 eV more negative than that of the O2p-level in a simple component metal oxide. This causes the narrowing of band gap energy, and then a response for visible light. Although the $InMO_4$-based materials are active for water splitting under visible light, their activities are usually low. In addition, no usage of these photocatalysts in gas–solid heterogeneous photocatalysis for decomposing organic pollutants has been reported. This is due to fact that the high-temperature-prepared solid phases typically possess a very small surface area (<1 m^2/g), making the surface-based gas–solid reactions awfully inefficient [20].

Instead of using $InMO_4$ directly as a visible-light-driven photocatalyst, we have explored the potential of the multicationic metal oxide as a stable inorganic sensitizer to activate titania [21,22]. As the electronic structures of $InMO_4$ matches well with that of TiO_2 (Scheme 1), an efficient surface charge separation between them is expectable [19]. This paper describes a much more sophisticated system in which building blocks of nanoscale $InVO_4$ and TiO_2 are integrated into mesoporous architecture. Such an architectural design offers the ultrahigh dispersion of sensitizer on a large-surface-area TiO_2 porous network. The physicochemical properties of the nanocomposite are also described. The visible-light-driven photoactiviy of the catalyst was investigated for the photocatalytic decomposition of some organic pollutants, such as benzene, cyclohexane, toluene ethylbenzene, and acetone. Meanwhile, because of high toxicity and environmental pertinacity, benzene was chosen as a main probe to test the toxic endurance and the structural stability of the photocatalyst upon visible light irradiation.

2. Experimental

2.1. Materials

$InCl_3$, V_2O_5, NaOH, cyclohexane, toluene ethylbenzene, and acetone were analytical grade and purchased from the Shanghai Chemical Co. SiO_2 (Alfa, specific surface = 144 $m^2\ g^{-1}$) and Benzene (Acros, spectrophotometric grade) were obtained from the Phentex Chemical Co. and the J&K Chemical Co., respectively. All reagents were used without further treatment.

2.2. Preparation of catalysts

The $InVO_4$-modified mesoporous nanocrystalline TiO_2 was prepared by a sol–gel method. Mixture was formed by adding a small amount of $InVO_4$ sol to TiO_2 sol, and then gelatinized by heating treatment. In a typical synthesis, a solution containing $InCl_3$ and $NaVO_3$ with a molar ratio of 1:2 was adjusted to pH 8.0 by adding NaOH. The solution was placed in a Teflon-lined stainless steel autoclave and then hydrothermally treated at 150 °C for 16 h. The resulting precipitate was washed with distilled water to remove impurities. The washed precipitate was dispersed in a butyl ethanol solution. This mixture was distilled for 6 h to form a homogeneous $InVO_4$ sol solution. Titanium tetraisopropoxide was hydrolyzed under acidic conditions and the resulting suspension was dialyzed to pH of ca. 4 and then form a transparent TiO_2 sol [23]. The sols of $InVO_4$ and TiO_2 (the initial ratio of $InVO_4$ to TiO_2 was fixed at 0.5 wt.%) were mixed, stirred for 48 h, and then heated to remove solvents. The resultant xerogels were calcined at 450 °C for 3 h, and then grinded and sieved to obtain particulates of the 0.21–0.25 mm size. As a comparison, pure TiO_2, $InVO_4$, $InVO_4/SiO_2$ and In (or V)-doped TiO_2 were also prepared. The synthesis process of $InVO_4/SiO_2$ was similar to that of $InVO_4/TiO_2$. In (or V)-doped catalyst was prepared by dropping the $InCl_3$ (or $NaVO_3$) solution to TiO_2 sols. The post heating treatment process was also similar to that of $InVO_4/TiO_2$. N-doped TiO_2 catalyst ($TiO_{2-x}N_x$) was prepared by a dry method [5]. The as-prepared TiO_2 sol was dried at 60 °C for 24 h, then heated at 450 °C in an alumina tube reactor under dry NH_3 gas flow for 3 h.

2.3. Characterization

In this paper, it was the 0.5 wt.% $InVO_4$ in TiO_2 that was used constantly for the physical characterization. X-ray diffraction (XRD) analysis was performed using a Bruker D8 Advance diffractometer with CuKα radiation. The crystallite size of anatase was calculated from the peak half-width by using the Scherrer equation with corrections for instrumental line broadening [24]. The phase content of a sample was calculated from the integrated intensities of anatase (101), rutile (110) [25]. Transmission electron microscopy (TEM) and high-resolution transmission electron microscopy (HRTEM) were recorded on a JEOL 2010F microscope operated at a 200 kV accelerating

voltage to elucidate the mesostructure of the samples. Nitrogen adsorption–desorption isothermals for the specific surface area and pore volume of the samples were collected at 77 K using Micromeritics ASAP 2010 equipment. Prior to adsorption experiments, the samples were degassed to 10^{-5} Torr at 573 K for 4 h. UV-vis diffuse reflectance spectra (DRS) of samples were recorded on a Varian Carry 500 Scan, equipped with an integrating sphere attachment. The reflectance data were converted to the F(R) values according to Kubelka–Munk theory [26]. X-ray photoelectron spectroscopy (XPS) analysis was conducted on a VG Scientific ESCASAB Mark II spectrometer using Al Ka as the radiation source (hv = 1486.6 eV). The catalysts were crushed and pressed into the sample holder on a double-side glue tape. The samples were degassed and the residual vacuum in the sample chamber was maintained at 2×10^{-9} Torr during analysis. Charging effects were calibrated by C1s line at 284.8 eV. Ultraviolet photoelectron spectra (UPS) were carried out in an ultrahigh vacuum (UHV) apparatus of a VG ADES-400 electron energy spectrometer with a base pressure of $<2 \times 10^{-8}$ Pa. The apparatus contains an argon-ion gun with a hot filament, a fixed ultraviolet source, and a semispherical deflector analyzer (SDA). The sample stage can be rotated along the polar axis. The sample was cleaned several times by argon-ion sputtering (1000 eV, 30 min) to remove surface contamination. The UPS was measured using He I excitation (21.2 eV) and recorded with a constant pass bias of −5 eV. The overall resolution of the measurement is 0.05 eV. All of the measurements are carried out at ambient temperature. Electron paramagnetic resonance (EPR) signals of the radicals spin-trapped by DMPO were recorded with a Bruker ESP 300E spectrometer after 3 min irradiation of methanol or aqueous dispersions (catalyst, 4 g L^{-1}; DMPO, 0.05 M). The irradiation source (λ = 532 nm) was a Quanta-Ray Nd:YAG pulsed (10 Hz) laser system. The settings for the EPR spectrometer were: center field = 3480 G, microwave frequency = 9.79 GHz and power = 5.05 mW. Oxygen adsorption capacities of $InVO_4$ and $InVO_4/TiO_2$ were investigated by temperature-programmed desorption of oxygen (O_2-TPD) using a volumetric flow apparatus (Autochem 2910, Micrometrics) with helium as a carrier gas. Samples were heated in situ to 300 °C with a heating rate of 10 °C/min under a 50 mL/min 100% O_2 flow, kept at 300 °C for 1 h, cooled to 25 °C with a rate of 2 °C/min under flowing O_2, and flushed with 50 mL/min helium for 30 min. The O_2 desorption heating rate was 10 °C/min from 50 to 700 °C. The analyses of the desorbed gases were performed continuously with a quadrupole mass spectrometer (Balzers OminiStar Thermo 300). For quantitative measurements, the mass spectrometer was calibrated for the O_2 signal.

2.4. Reactivity measurements

The measurement of photocatalytic activity was carried out in a fixed-bed quartz reactor with volume of 1 ml and operated at ambient conditions [23]. The light resource was a 500 W Xe-arc lamp equipped with an IR-cutoff filter and an UV-cutoff filter. The pass-band of the coupled filters was identified as 450 nm ≤ λ ≤ 900 nm by the UV-vis spectrophotometer described above. Organic pollutant (e.g. benzene, toluene, cyclohexane, acetone or ethylbenzene) fixed at a certain concentration was supplied by bubbling with oxygen in nitrogen from a gas cylinder, then continually fed to typical 1.2 g of catalyst at a total flow-rate of 50 cm^3 min^{-1}. The temperature of the reaction was controlled at room temperature by an air-cooling system. The effluent gas was analyzed by an online gas chromatograph (HP6890) equipped with a flame ionization detector (FID), a thermal conductivity detector (TCD), and a Porapak R column. The concentrations of organic pollutants and carbon dioxide were determined by using the FID and TCD detectors, respectively. The gas chromatograph was calibrated using known concentrations of reactants and carbon dioxide. Before an activity measurement, the adsorption/desorption equilibrium of reactant gas on sample was obtained after 5 h in dark.

3. Results and discussion

3.1. Textural and optical properties

The N_2 adsorption–desorption of the $InVO_4/TiO_2$ sample is found to be of type IV isotherms, and the pore size distribution plot shows a narrow pore size distribution with average pore diameter of 10 nm (Fig. 1). These results indicate that the $InVO_4/TiO_2$ is a mesoporous solid [27]. The BET specific surface area and pore volume (90 m^2/g, 0.28 cm^3/g) of the $InVO_4/TiO_2$ are larger than those of the pure TiO_2 (62 m^2/g, 0.21 cm^3/g), which suggests that the addition of $InVO_4$ inhibits the collapse of mesoporous structure during the thermal treatment. In addition, the BET specific surface area and pore volume of $TiO_{2-x}N_x$ is 67 m^2/g and 0.22 cm^3/g, respectively.

The porous nature of $InVO_4/TiO_2$ is also characterized by transmission electron microscopy as shown in Fig. 2a, where a interconnected fine particulate morphology is observed, indicating the inter-particle porosity [28]. Fig. 2b shows the nanocrystalline nature of $InVO_4/TiO_2$ as examined by high-resolution TEM. The fringes appearing in the micrographs allow for the identification of the crystallographic spacing of TiO_2 and $InVO_4$. The fringes of d = 3.5 Å and d = 2.8 Å observed match

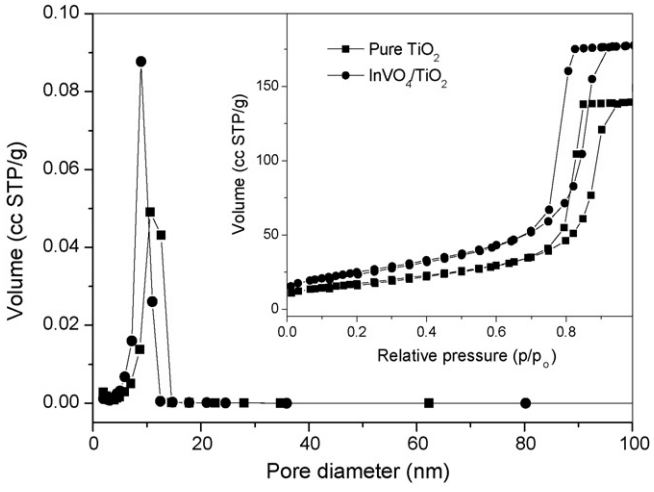

Fig. 1. Nitrogen-sorption isotherms and the pore size distribution plots for TiO_2 and $InVO_4/TiO_2$.

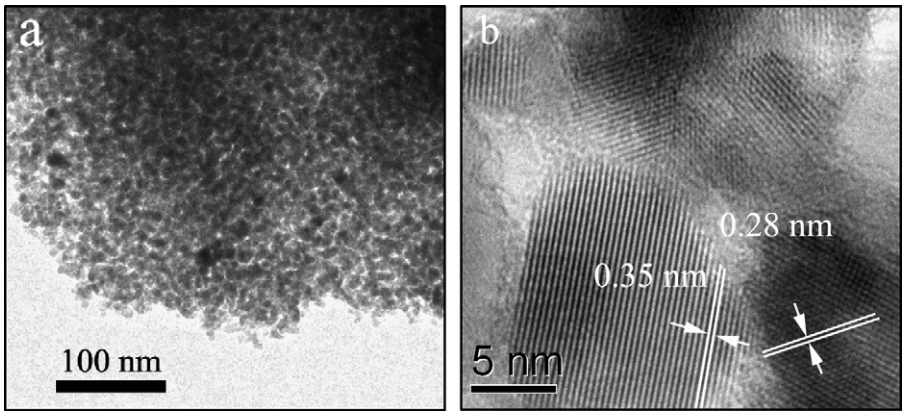

Fig. 2. TEM image of $InVO_4/TiO_2$ photocatalyst, and (b) HRTEM image of the sample.

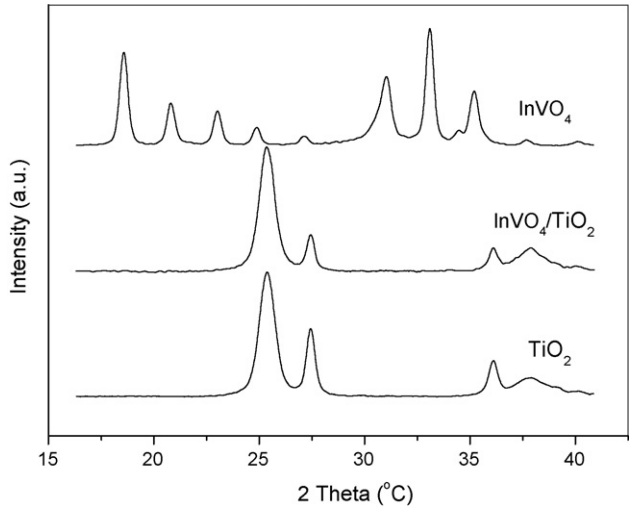

Fig. 3. XRD patterns of $InVO_4$, TiO_2 and $InVO_4/TiO_2$.

that of the (101) and (200) crystallographic planes of anatase TiO_2 and $InVO_4$ orthorhombic phase, respectively, indicating the existence of $InVO_4/TiO_2$ heterogeneous junctions. Interestingly, this kind of heterogeneous junction has almost not been observed for $InVO_4/TiO_2$ sample without heat treatment. The disappearing of such junctions also occurs for the $InVO_4$–TiO_2 sample prepared by mechanically mixing. It should be noted that such heterogeneous junctions is generally detected during TEM measurements for $InVO_4/TiO_2$ sample with heat treatment. It seems that the strong interaction between the two composites is formed in the thermal treatment process, and this may be one of the reasons that account for the discrepant photoactivity of the samples described below.

Fig. 3 shows the XRD patterns of $InVO_4/TiO_2$. As a comparison, the XRD patterns of the as-prepared pure $InVO_4$ with a character of orthorhombic $InVO_4$ (ICSD010431) and the pure TiO_2 with main components of anatase (A) and rutile (R) are also presented. For the sample with 0.5% $InVO_4$ in TiO_2, no distinct peak corresponding to $InVO_4$ is observed. This is because the amount of $InVO_4$ is so small that it is beyond the detection of XRD or $InVO_4$ exists in a highly dispersed form in the porous TiO_2 host. In addition, when the amount of $InVO_4$ in TiO_2 exceeds 2%, the peaks corresponding to orthorhombic $InVO_4$ appear. This confirms the existence of $InVO_4$ in TiO_2. In this investigation, the peak at $2\theta = 25.4 \pm 0.1^\circ$ is considered as anatase (1 0 1), and the peak at $2\theta = 27.4 \pm 0.1^\circ$ is considered as rutile (1 1 0). The calculated results of the weight percentage of crystal phase (W) for the samples are shown in Table 1. Obviously, a decrease in W_R value and an increase in W_A are detected for $InVO_4/TiO_2$, compared with TiO_2. It shows that adding small amount of $InVO_4$ remarkably suppresses the phase transformation of TiO_2 from anatase to rutile phase. Kozlowski et al. [29] reported the opposite results relating to phase transformation of TiO_2 doped by V element. It might be concluded that the phase transformation of $InVO_4/TiO_2$ is not due to the V doping. This implies that doping V into TiO_2 lattice is unlikely in $InVO_4/TiO_2$ sample. On the basis of XRD results, the crystal size (D) and the "d" space values between the crystal planes of $InVO_4/TiO_2$ sample were also presented. It shows no distinct changes in the crystal size and the "d" space values are observed for the anatase or rutile phase. This confirms that the In or V species doesn't dope into the lattice of TiO_2.

Fig. 4 shows the UV-visible DRS of the TiO_2, $InVO_4$, $InVO_4/TiO_2$ and $TiO_{2-x}N_x$ samples. Compared to that (~400 nm) of pure TiO_2, the absorption onset of $InVO_4/TiO_2$ is estimated at 540 nm, with a red shift of 140 nm. Obviously, the absorption of $InVO_4/TiO_2$ in the visible light range is due to the contribution of $InVO_4$. The absorption onset of $InVO_4$ is estimated at 590 nm corresponding to the band gap of 2.1 eV,

Table 1
The crystal size (D), the weight percentage of the crystal phase (W), and the distance between the crystal planes of TiO_2 modified by $InVO_4$

Sample	D_{101} (nm)	W_A (%)	d_{101} (nm)	D_{110} (nm)	W_R (%)	d_{110} (nm)
TiO_2	10.8	62.8	0.3516	21.5	37.2	0.3248
$InVO_4/TiO_2$	10.7	74.5	0.3516	21.1	25.5	0.3248

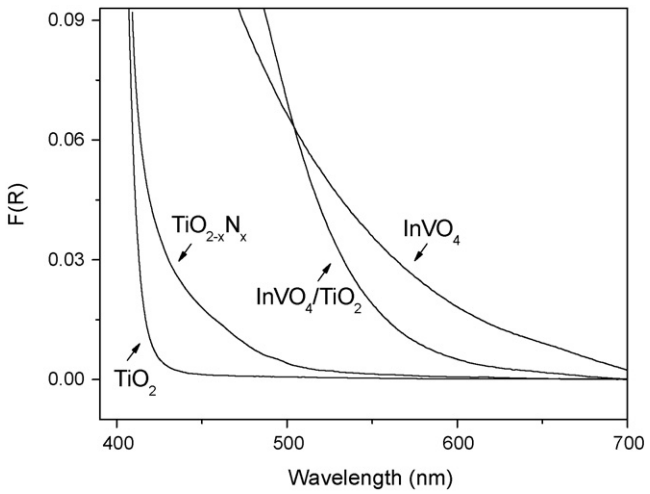

Fig. 4. Visible light absorption spectra of TiO_2, $InVO_4$, $InVO_4/TiO_2$ and $TiO_{2-x}N_x$.

which is in agreement with the previous report [19]. As a result of the modification of $InVO_4$ to TiO_2, it seems that $InVO_4$ may photosensitize TiO_2 in visible light. This permits the novel photocatalyst to respond to a wide range of solar spectrum. This light-responsive range is much wider than that of $TiO_{2-x}N_x$ photocatalyst (<500 nm), which well agrees with the reported value for the N-doped TiO_2 system [5].

3.2. Surface chemical composition and electronic state

XPS analysis was carried out to determine the surface chemical composition of the catalysts and the valence states of various species present therein. The XPS measurement also confirms the incorporation of $InVO_4$ with TiO_2 (Fig. 5). The analysis of the In3d and V2p core lines of the as-prepared sample clear indicates the presence of In^{3+} and V^{5+} oxidation states (445.0 eV and 452.6 eV for In3d, 516.7 eV and 524.4 eV for V2p) [30]. This suggests no changes of the oxidation state of In and V occur at the surface during the thermal treatment of $InVO_4/TiO_2$ sample. Moreover, the core lines of Ti2p are fixed at 458.9 eV and 465.0 eV for both TiO_2 and $InVO_4/TiO_2$, and no shift of the Ti2p core lines is detected for the $InVO_4$ doping, implying no strong interaction among Ti, In and V atoms of $InVO_4/TiO_2$.

3.3. Determination of electronic band position

Theoretically, the electronic structure of $InVO_4$ had been calculated by density functional theory [19]. The DFT calculations revealed that the conduction band of $InVO_4$ consists of

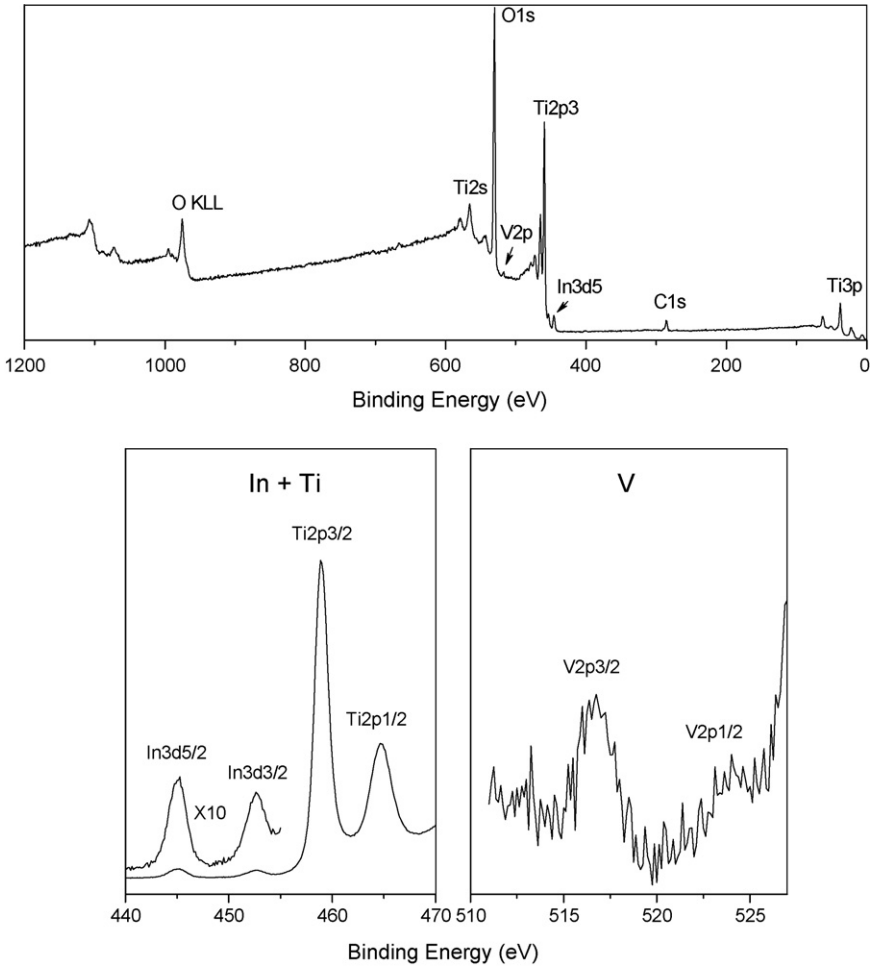

Fig. 5. X-ray photoelectron spectra (XPS) of $InVO_4/TiO_2$.

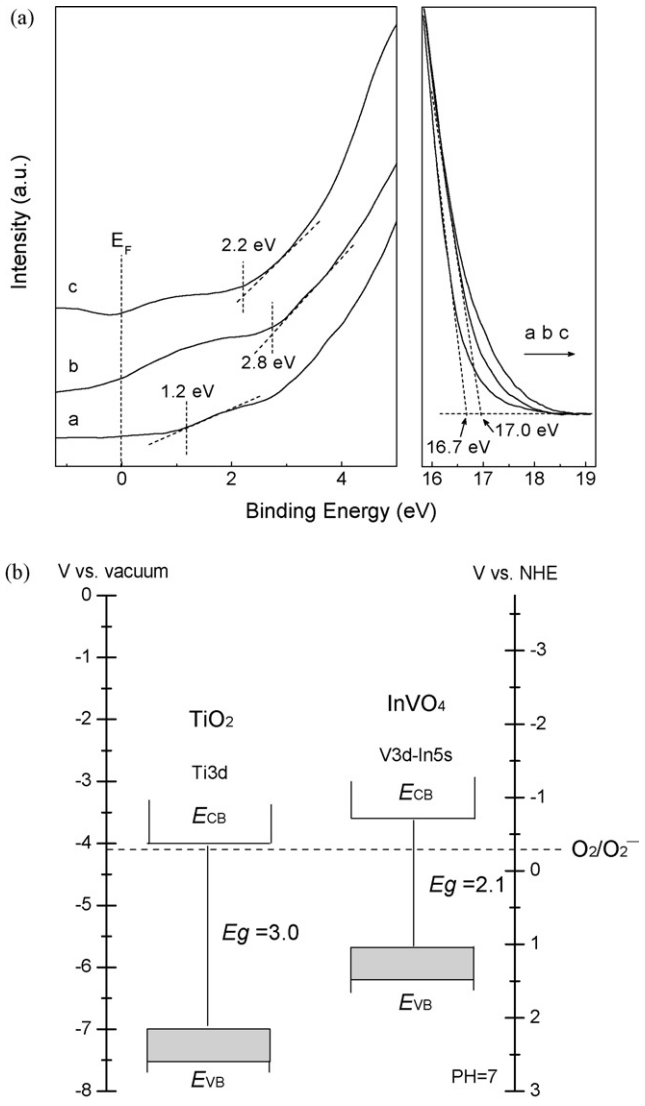

Fig. 6. (a) Ultraviolet photoelectron spectra (UPS) of $InVO_4$ (a), TiO_2 (b) and $InVO_4/TiO_2$ (c). (b) Position of the E_{CB} and E_{VB} for TiO_2 and $InVO_4$ on the absolute vacuum energy scale and with respect to normal hydrogen electrode (NHE). The relationship between the absolute vacuum energy (E_{abs}) and the normal electrode potential (E°) is expressed as follows: $E_{abs} = -E^{\circ} - 4.44$ (at 298 K). $E^{\circ}(O_2/O_2^{\bullet -})$ of −0.33 V is taken as a reference.

hybridized orbitals of V3d and In5s, and the valance band (VB) is composed of 2p orbitals of O atoms. Furthermore, to determine the possibility of $InVO_4$-sensitized TiO_2, UPS is a useful technique for this situation [31,32], because the energy bands for the two composites can be well established. UPS spectra of $InVO_4$, TiO_2 and $InVO_4/TiO_2$ measured at sample biases (−5 v) are shown in Fig. 6a. According to the spectrum a, the valence band maximum (E_{VB}) of $InVO_4$ is located at ca. −5.7 eV (versus vacuum) determined by fitting a straight line into the leading edge. The secondary electron onset (SO) on the right side of the spectrum is 16.7 eV. The work function of $InVO_4$ was calculated to be 4.5 eV by subtracting the SO position of the He I UPS spectrum from the excitation energy (21.2 eV). The corresponding Fermi level (E_F) is located at −4.5 eV (versus vacuum). Determined by the UV-visible DRS, the value of band gap (E_{BG}) is 2.1 eV for $InVO_4$. Therefore, the conduction band minimum (E_{CB}) of $InVO_4$ is located at ca. −3.6 eV (versus vacuum). Similarly, the value of E_{BG}, E_{VB}, E_F and E_{CB} determined by UV-visible DRS and UPS are summarized in Table 2. The results reveal that the E_{CB} of TiO_2 is located at −4.0 eV (versus vacuum), which is more negative than that of $InVO_4$. (Fig. 6b) Obviously, the difference of E_{CB} between $InVO_4$ and TiO_2 allows the transfer of electron from the CB of $InVO_4$ to that of TiO_2, making the $InVO_4$ an efficient 'electron pump' for the intrinsic visible-light-sensitization of TiO_2. As expected, based on the E_{BG} value of 2.3 eV from UV-visible DRS, the result of UPS for $InVO_4/TiO_2$ indicates that and the apparent E_{CB} and E_{VB} of $InVO_4/TiO_2$ are −4.1 eV and −6.4 eV (versus vacuum), respectively. On the basis of the relationship between the absolute vacuum energy (E_{abs}) and the normal electrode potential (E°), the apparent E_{CB} of $InVO_4/TiO_2$ is −0.34 V (versus NHE), which is almost the same as that of $E^{\circ}(O_2/O_2^{\bullet -})$ (−0.33 V versus NHE) [33]. Therefore, it is possible for the adsorption oxygen to capture electron from the CB of $InVO_4/TiO_2$, resulting in an active oxygen species ($O_2^{\bullet -}$), subsequently leading to VOCs decomposition.

Table 2
Band energies of $InVO_4$, TiO_2 and $InVO_4/TiO_2$ by UV-visible DRS and UPS

Sample	E_{BG} (eV)	E_F (eV)	E_{VB} (eV)	E_{CB} (eV)
$InVO_4$	2.1	−4.5	−5.7	−3.6
TiO_2	3.0	−4.2	−7.0	−4.0
$InVO_4/TiO_2$	2.3	−4.2	−6.4	−4.1

3.4. Photocatalytic activity

Fig. 7 displays the visible light activity of $InVO_4/TiO_2$ for decomposing benzene in air. The result demonstrates the high photocatalytic performance and the good stability in the photocatalytic process. The conversion of benzene and the production of CO_2 are observed at steady state after ca. 1 h of illumination (Fig. 7a). The reaction was allowed to continue for 12 h and the $InVO_4/TiO_2$ generated 147.5×10^{-3} mol of CO_2 per gram of catalyst, by photodecomposition of 77.5×10^{-3} mol of benzene in air. The catalyst turnover number recorded within 12 h works out to be 11.8 mol (CO_2) per mol ($InVO_4/TiO_2$), indicating that the observed benzene photooxidation is indeed catalytic. It is noted that the benzene oxidation isn't stoichiometric, suggesting that the benzene with stable aromatic structure is partially oxidized. The experiment was also carried out for five runs to examine the stability of the catalyst under visible light irradiation as shown in Fig. 7b. In the first run, the photocatalytic conversion of benzene was 48.7%, and the amount of CO_2 produced from the reactions was up to 188 ppm. When the steady state was reached, the conversion was maintained at ca. 46.5% for the following four runs, and the production of CO_2 was ca. 180 ppm. Additionally, no benzene degradation and no CO_2 evolution in the blank test (no photocatalyst) under visible light irradiation, confirmed that the decompositions of the typical environmental pollutant occurred through photocatalysis and that it self-photolysis could be neglected.

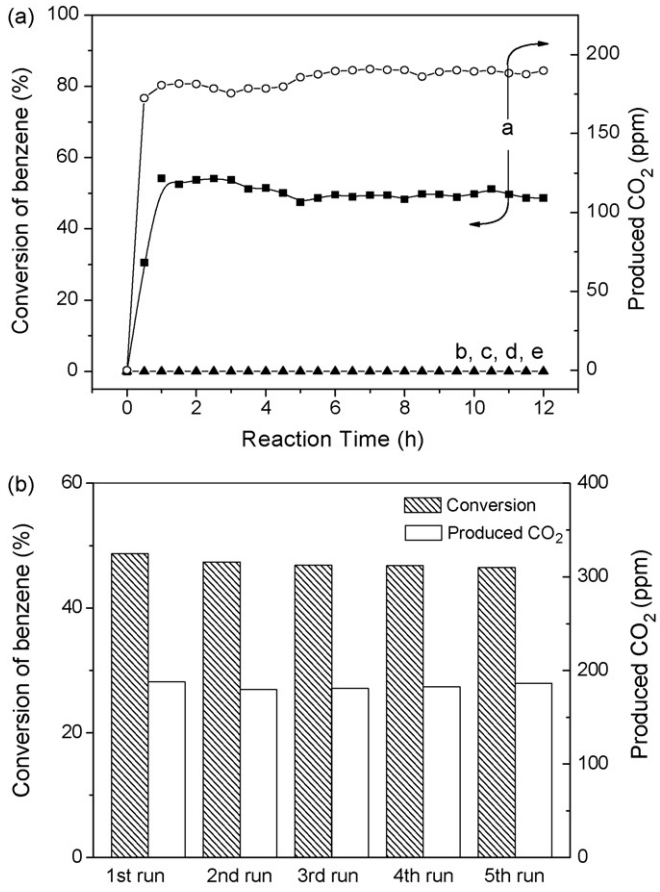

Fig. 7. (a) Photodegradation of benzene (215 ppm) on $InVO_4/TiO_2$(a) under visible light irradiation. The activity of $TiO_{2-x}N_x$(b), $InVO_4$(c), TiO_2(d) and $InVO_4/SiO_2$ (e) samples are also measured for comparison. (b) Photodegradation of benzene (215 ppm) on $InVO_4/TiO_2$ photocatalysts during repetition operation upon visible light irradiation.

To further understand the photocatalytic performance of the $InVO_4/TiO_2$ catalyst, the nitrogen-doped TiO_2 ($TiO_{2-x}N_x$) visible light photocatalyst was chosen for a comparison. Noticeably, complete deactivation was rapidly observed during the photocatalytic degradation of benzene, resulting in the sample discoloration from yellowish to chocolate brown (Fig. 7a). It shows that some reaction intermediates are strongly adsorbed on the catalyst surface and make it deactivated. On the contrarily, no deactivation and discoloration were observed for $InVO_4/TiO_2$ of dark red even after the catalyst was evaluated for 60 h.

As a comparison, measurements were also carried out to study the activity of pure TiO_2, $InVO_4$ and $InVO_4/SiO_2$ under visible light irradiation (Fig. 7a). As a result, no degradation of benzene was observed in these cases. It implies that no photocatalytic degradation of benzene takes place on TiO_2 or $InVO_4$ alone. Moreover, no photocatalytic activity under visible light irradiation can be found when testing the activity of In_2O_3/TiO_2, V_2O_5/TiO_2, $(In_2O_3–V_2O_5)/TiO_2$ towards benzene decomposition. In addition, there is no decomposition of benzene occurred when mixing the two powders of pure TiO_2 and $InVO_4$ together simply. These results suggest that the interaction of $InVO_4$ with TiO_2 is required to activate TiO_2 for visible light photocatalysis and which contributes to the high activity and durability of $InVO_4/TiO_2$ for organic decomposition. We also found that the $InVO_4/TiO_2$ must be sintered at temperatures between 300 °C and 500 °C for achieving high photocatalytic performance under visible light irradiation. The optimum sintering temperature was 450 °C. Certainly, a high temperature is important for the strong interaction between $InVO_4$ and TiO_2, which is in favor of photogenerated-carrier transfer. However, the specific surface area of $InVO_4/TiO_2$ will also decrease for the increasing temperature. Compared with the sample sinter at 500 °C, the BET specific surface area of $InVO_4/TiO_2$ remarkably decreases to 53 $m^2\,g^{-1}$. This may lead to a decrease in photocatalytic performance.

The effect of $InVO_4$ concentration in TiO_2 on the visible light activity of $InVO_4/TiO_2$ was also investigated towards benzene degradation (Fig. 8). In the absence of $InVO_4$, the conversion was zero. The best concentration of $InVO_4$ is 0.5%. The activity of $InVO_4/TiO_2$ gradually decreased when the concentration of $InVO_4$ was increased from 0.5 to 10%, at which the photocatalyst was virtually inactive for benzene decomposition. The same trend can be found when photocatalytic activity is measured for ethylene or other organic pollutants. It is known that an ideal sensitizer should be homogeneously attached to the semiconductor surface as small particles [34]. Such directly connected sensitizers are more effective in injecting electrons into the semiconductor as compared to those in outer layers. When the concentration of $InVO_4$ is 0.5%, $InVO_4$ is highly dispersed on the high-surface-area TiO_2 as small nanoparticles, as indicated by the absence of XRD signal in the sample. When the concentration of $InVO_4$ increases, more and more TiO_2 will be shielded by the overgrowth $InVO_4$. Since the pure $InVO_4$ is inactive toward benzene degradation, the shielding effect may cause the reduction in the photosensitization efficiency of $InVO_4$.

$InVO_4/TiO_2$ photocatalyst also exhibited good photocatalytic performance for other VOCs degradation under visible light irradiation. As shown in Fig. 9, the conversion of the target reactants and the production of CO_2 are measure at steady state after PCO for 12 h. The photocatalytic conversion of cyclohexane, ethylbenzene, toluene and acetone are 62%, 64%, 57% and 31%, respectively. The corresponding CO_2 produced are 366 ppm,

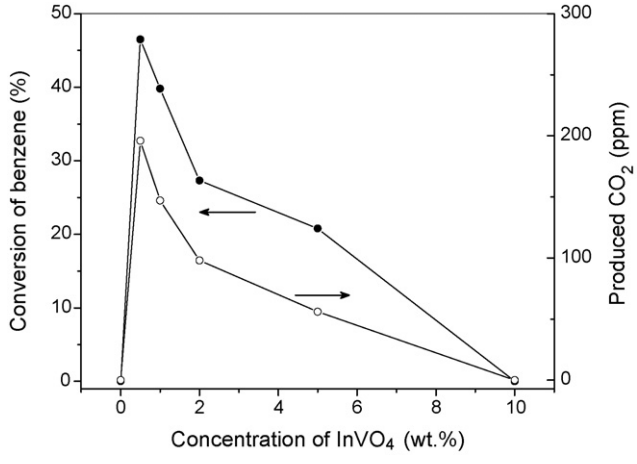

Fig. 8. Photocatalytic conversion of benzene on visible-light-driven $InVO_4/TiO_2$ as a function of $InVO_4$ concentration in the catalyst.

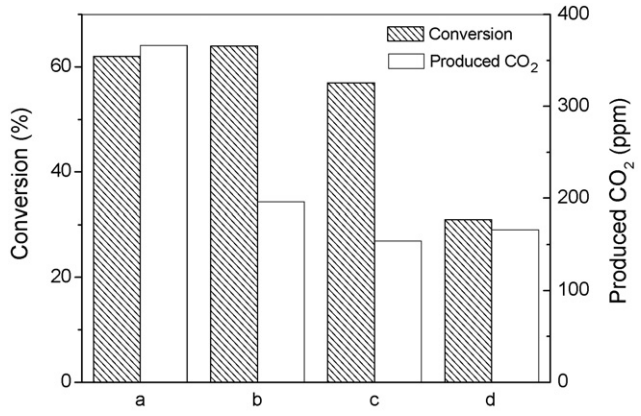

Fig. 9. Photooxidation of other VOCs on $InVO_4/TiO_2$ irradiated by visible light: (a) cyclohexane (250 ppm), (b) ethylbenzene (200 ppm), (c) toluene (200 ppm) and (d) acetone (500 ppm).

196 ppm, 154 ppm and 166 ppm, respectively. Similarly, no deactivation was detected on the $InVO_4/TiO_2$ photocatalyst. In addition, no obvious degradation of the target reactants can be also detected on $InVO_4$ samples.

3.5. Photochemical processes

In general, it is known that the photocatalytic reactions proceed mainly by the contributions of active oxygen species, such as $O_2^{\bullet -}$, $OH^{\bullet}$ and H_2O_2 [2,35,36]. Particularly, since the reaction ability of $OH^{\bullet}$ is high enough to attack any organic molecules, it has been assigned as a key species in the mineralization of many hazardous chemical compounds. Thus, to probe the nature of the reactive oxygen species generated during the visible light irradiation of $InVO_4/TiO_2$ system, EPR spin-trap technique (with DMPO) is used to monitor the intermediate radicals in the system. It has been reported that the superoxide radical anion ($O_2^{\bullet -}$) remains stable in methanol medium and the hydroxyl radical ($OH^{\bullet}$) can be detected in aqueous medium [37]. Consequently, the EPR spectra of DMPO–$O_2^{\bullet -}$ and DMPO–$OH^{\bullet}$ adducts were investigated in irradiated methanol and aqueous dispersions, respectively.

Firstly, we recorded EPR spectra for pure TiO_2 and $InVO_4$ illuminated with visible light (532 nm), respectively. Neither DMPO–$O_2^{\bullet -}$ nor DMPO–$OH^{\bullet}$ adducts are detected by EPR for the TiO_2 or $InVO_4$ alone. Since the optical absorption edge of TiO_2 is 387 nm, the visible light (532 nm) cannot induce the formation of reactive radicals such as $O_2^{\bullet -}$ and $OH^{\bullet}$. Compared with TiO_2, the narrower band-gap of pure $InVO_4$ can be activated theoretically by the visible light as shown in reaction 1. However, it seems that the separation of photoinduced electron-hole pairs on pore $InVO_4$ is too inefficient to generate enough superoxide radical anion for EPR detection. This is also supported by our experiment that $InVO_4$ are virtually inactive for the degradation of benzene under visible light irradiation (Fig. 7a).

Interestingly, in the case of $InVO_4$-sensitized TiO_2, six characteristic peaks of the DMPO–$O_2^{\bullet -}$ adducts are observed as shown in Fig. 10. No such signals were detected in the dark or the blank test. As known above (Fig. 6 and Table 2), CB potential

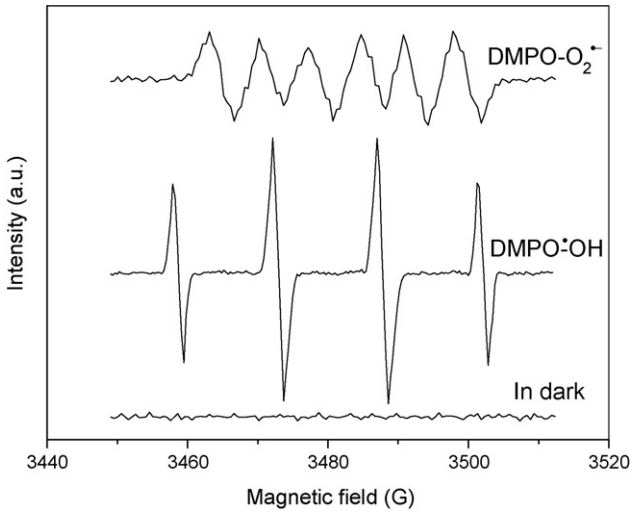

Fig. 10. EPR spectra of radical adducts with DMPO in $InVO_4/TiO_2$ dispersions: (a) DMPO-$O_2^{\bullet -}$ formed in irradiated methanol dispersions; (b) DMPO-$^{\bullet}$OH in irradiated aqueous dispersions; (c) sample in methanol or aqueous dispersion before irradiation.

of $InVO_4$ is ca. −0.84 (V versus NHE), whereas the CB potential of TiO_2 is ca −0.44 (V versus NHE). These data point to an interfacial electron-transfer process between the $InVO_4$ and TiO_2 particles. The TiO_2 may act as an active center for hindering the recombination of photoinduced electron-hole pairs and transfers electron to absorbed oxygen through its CB, subsequently resulting in a yield of $O_2^{\bullet -}$ radicals (reactions 2 and 3). The EPR analysis confirmed that $O_2^{\bullet -}$ radicals are formed much more efficiently on $InVO_4/TiO_2$ than on naked $InVO_4$ alone. Certainly, since the bottom of CB in $InVO_4$ locates more negative than that in TiO_2, the photogenerated electrons in $InVO_4$ may directly reduce the absorbed oxygen to form $O_2^{\bullet -}$ radicals. However, compared to the absorption of oxygen for $InVO_4/TiO_2$ (17.5 mL g^{-1}), the quantity of oxygen absorbed on pure $InVO_4$ is very small (0.2 mL g^{-1}). Moreover, the concentration of $InVO_4$ on the surface of $InVO_4/TiO_2$ is poorly low (0.5 wt.%), so little oxygen is absorbed on the $InVO_4$ particles. It means the production of $O_2^{\bullet -}$ radicals are inefficient for the electron transfer between the CB of $InVO_4$ and its absorbed oxygen, which agrees well with the result of EPR analyses. Namely, the $O_2^{\bullet -}$ radicals found in the $InVO_4/TiO_2$ photocatalytic system may be formed by the injected electron to oxygen through the CB of TiO_2.

$$InVO_4 + hv \rightarrow InVO_4(h^+ + e^-) \quad (1)$$

$$InVO_4(h^+ + e^-) + TiO_2 \rightarrow InVO_4(h^+{}_{VB}) + TiO_2(e^-{}_{CB}) \quad (2)$$

$$TiO_2(e^-{}_{CB}) + O_2 \rightarrow TiO_2 + O_2^{\bullet -} \quad (3)$$

Moreover, the DMPO–$OH^{\bullet}$ adducts with the characteristic 1:2:2:1 quartet pattern ($\alpha_N = \beta_H = 1.48$ mT [38,39]) were also observed for $InVO_4/TiO_2$ in the EPR experiments. In addition, no such signals were also detected in the dark or the blank test. Noted that it is too weak for the hole ($h^+{}_{VB}$) of $InVO_4$

(+1.26 V versus NHE) to oxide hydroxyl to form $OH^{\bullet}$ radical ($E^0_{OH^{\bullet}/OH^-} = +2.38$ V versus NHE [33]) under visible light irradiation. It is proposed that the generation of $OH^{\bullet}$ radical may originate from $O_2^{\bullet-}$ radical as below (reactions 4 and 5). Although, it is impossible to generate $OH^{\bullet}$ radical through the direct oxidation of oxide hydroxyl, the photogenerated hole in $InVO_4$ can easily activate some unsaturated organic pollutants (e.g. benzene), leading to a subsequent decomposition. Certainly, the hole (h^+_{VB}) of $InVO_4$ can also consume $O_2^{\bullet-}$ to form O_2 (reaction (6)).

$$O_2^{\bullet-} + TiO_2(e^-_{CB}) + 2H^+ \rightarrow TiO_2 + H_2O_2 \quad (4a)$$

$$2O_2^{\bullet-} + 2H^+ \rightarrow O_2 + H_2O_2 \quad (4b)$$

$$H_2O_2 + TiO_2(e^-_{CB}) \rightarrow OH^{\bullet} + OH^- + TiO_2 \quad (5)$$

$$InVO_4(h^+_{VB}) + O_2^{\bullet-} \rightarrow InVO_4 + O_2 \quad (6)$$

In this way, active oxygen species ($O_2^{\bullet-}$, $OH^{\bullet}$ and H_2O_2) are generated from the sensitization of TiO_2 with $InVO_4$, subsequently leading to the oxidation of organic compounds. Obviously, the photosensitizer of $InVO_4$ distinctly differs from the traditional organic dyes, which are known to inevitably lose their visible-light-responsive functions due to the self-photocorrosion or self-photodegradation. In the case of photosensitization with $InVO_4$, high visible-light-induced photocatalytic activity and superior stability can be observed on $InVO_4/TiO_2$ catalyst.

4. Conclusions

When modified by small quantities of $InVO_4$ (0.5 wt.%), the mesoporous TiO_2 catalyst is a stable and relative efficient system for the visible light photodegradation of VOCs. The good durability of the photocatalysts is due to the stable sensitizer of $InVO_4$ under visible light irradiation. The relative high photocatalytic performance of $InVO_4/TiO_2$ is interpreted by the generation of superoxide radical anion (e.g. $O_2^{\bullet-}$ and $OH^{\bullet}$) under visible light irradiation, thereby leading to the efficient decomposition of VOCs.

Acknowledgments

This work was financially supported by the National Natural Science Foundation of China (20473018, 20573020, 20537010 and 20603007), Key Foundation of Science and Technology of MOE, China (03061 and JA02138), and the Natural Science Foundation of Fujian Province (2006J0160). The authors thank Prof. S.N. Bao of Zhejiang University for the UPS analysis.

References

[1] M.A. Fox, M.T. Dulay, Chem. Rev. 93 (1993) 341.
[2] M.R. Hoffmann, S.T. Martin, W. Choi, D.W. Bahnemannt, Chem. Rev. 95 (1995) 69.
[3] Z.G. Zou, J.H. Ye, K. Sayama, H. Arakawa, Nature 414 (2001) 645.
[4] M. Gratzel, Nature 414 (2001) 338.
[5] R. Asahi, T. Morikawa, T. Ohwaki, K. Aoki, Y. Taga, Science 293 (2001) 269.
[6] S. Khan, M. Al-Shahry, W.B. Ingler, Science 297 (2002) 2243.
[7] I. Tsuji, H. Kato, A. Kudo, Angew. Chem. Int. Ed. 44 (2004) 2.
[8] K. Maeda, T. Takata, M. Hara, N. Saito, Y. Inoue, H. Kobayashi, K. Domen, J. Am. Chem. Soc. 127 (2005) 8286.
[9] W. Zhao, W.H. Ma, C.C. Chen, J.C. Zhao, Z.G. Shuai, J. Am. Chem. Soc. 126 (2004) 4782.
[10] L. Zang, W. Macyk, C. Lange, W.F. Maier, C. Antonius, D. Meissner, H. Kisch, Chem. Eur. J. 6 (2000) 379.
[11] D. Dvoranova, V. Brezova, M. Mazura, M.A. Malati, Appl. Catal. B 37 (2002) 91.
[12] A. Sclafani, L. Palmisana, G. Marcy, A. Venezia, Sol. Energy Mater. Sol. C 51 (1998) 203.
[13] J.C. Yang, Y.C. Kim, Y.G. Shul, C.H. Shin, T.K. Lee, Appl. Surf. Sci. 121–122 (1997) 525.
[14] U. Bach, D. Lupo, P. Comte, J.E. Moser, F. Weissortel, J. Salbeck, H. Spreitzer, M. Gratzel, Nature 395 (1998) 583.
[15] J.C. Yu, L. Wu, J. Lin, P.S. Li, Q. Li, Chem. Commun. (2003) 1552.
[16] J.H. Tang, Z.G. Zou, J.H. Ye, Chem. Mater. 16 (2004) 1644.
[17] M. Oshikiri, J.H. Ye, Z.G. Zou, G. Kido, J. Chem. Phys. 117 (2002) 7313.
[18] M. Oshikiri, M. Boero, J. Ye, F. Aryasetiawan, G. Kido, Thin Solid Films 445 (2003) 168.
[19] J.H. Ye, Z.G. Zou, H. Arakawa, M. Oshikiri, M. Shimoda, A. Matsushita, T. Shishido, J. Photochem. Photobiol. A Chem. 148 (2002) 79.
[20] J.W. Tang, Z.G. Zou, J.H. Ye, Angew. Chem. Int. Ed. 43 (2004) 4463.
[21] G.C. Xiao, D.Z. Li, X.Z. Fu, X.X. Wang, P. Liu, Chin. J. Inorg. Chem. 20 (2004) 195.
[22] G.C. Xiao, W.S. Lu, D.Z. Li, X.X. Wang, X.Z. Fu, Chin. J. Inorg. Chem. 21 (2005) 551.
[23] X. Fu, A. Walter, Q. Yang, M.A. Anderson, J. Catal. 168 (1997) 482.
[24] J. Liu, J.C. Yu, D. Lo, S.K. Lam, J. Catal. 183 (1999) 368.
[25] H. Zhang, J.F. Banfield, J. Phys. Chem. B 104 (2000) 3481.
[26] M. Anpo, T. Shima, S. Kodama, Y. Kubokawa, J. Phys. Chem. 91 (1987) 4305.
[27] S.J. Gregg, K.S.W. Sing, Adsorption, Surface Area and Porosity, Academic, London, 1997, pp. 111–194.
[28] H.M. Luo, C. Wang, Y.S. Yan, Chem. Mater. 15 (2003) 3841.
[29] R. Kozlowski, R.F. Pettifer, J.M. Thomas, J. Phys. Chem. 87 (1983) 5176.
[30] D. Briggs, M.P. Seah, Practical Surface Analysis Auger and X-ray Photoelectron Spectroscopy, vol. I, second ed., Wiley, New York, 1990.
[31] G. Liu, W. Jaegermann, J. He, V. Sundström, L. Sun, J. Phys. Chem. 106 (2002) 5814.
[32] W. Chun, A. Ishikawa, H. Fujisawa, T. Takata, J.N. Kondo, M. Hara, M. Kawai, Y. Matsumoto, K. Domen, J. Phys. Chem. 107 (2003) 1798.
[33] A.J. Bard, R. Parsons, J. Jordan, Standard Potentials in Aqueous Solution, Marcel Dekker, New York and Basel, 1985.
[34] J.J. He, G. Benko, F. Korodi, T. Polivka, R. Lomoth, B. Åkermark, L.C. Sun, A. Hagfeldt, V. Sundstrom, J. Am. Chem. Soc. 124 (2002) 4922.
[35] N. Serpone, E. Pelizzetti, H. Hidaka, in: D.F. Ollis, H. Al-Ekabi (Eds.), Photocatalytic Purification and Treatment of Water and Air, Elsevier, London, 1993, pp. 225–250.
[36] T. Hirakawa, Y. Nosaka, Langmuir 18 (2002) 3247.
[37] T. Wu, T. Lin, J. Zhao, H. Hidaka, N. Serpone, Environ. Sci. Technol. 33 (1999) 1379.
[38] W. Zhao, C. Chen, X. Li, J. Zhao, H. Hidaka, N. Serpone, J. Phys. Chem. 106 (2002) 5022.
[39] W.G. Wamer, J.J. Yin, R.R. Wei, Free Radic. Biol. Med. 23 (1997) 851.